Evaluation of Convolution Integrals at Late-times Revisited

Lager, Ioan E.; Stumpf, Martin; Vandenbosch, Guy A.E.; Antonini, Giulio

Important note
To cite this publication, please use the final published version (if applicable).
Please check the document version above.

Communication

Evaluation of Convolution Integrals at Late-Times Revisited

Ioan E. Lager, Martin Štumpf, Guy A. E. Vandenbosch, and Giulio Antonini

Abstract—The late-time evaluation of electromagnetic (EM) field quantities yielded by convolution integrals that combine Green's functions available at discrete time samples and strictly causal excitations is critically revisited. A typical situation is used for tracing the causes of the divergent late-time behavior that is often experienced. A framework combining a suitable integral partitioning with a polynomial approximation is shown to effectively guarantee the integrals' convergence. The formulation is validated via numerical experiments evidencing its accuracy and computational efficacy. The method is amenable to be used in a wide range of problems requiring the late-time evaluation of convolution integrals of the indicated type.

Index Terms—Convolution, late-time behavior, numerical analysis, polynomial approximation.

I. INTRODUCTION

Infinite integrals are prominently present in various approaches to solving the electromagnetic (EM) field equations. In particular, they are of critical relevance in (semi)analytical formulations making use of integral representations, with [1]–[3] being illustrative for the sustained efforts invested in the effective handling of the tail of such integrals.

Infinite integrals are important for the EM analysis of layered media that starting with Sommerfeld [4] relies on the use of Green's functions (see the overview in [5, Ch. 2]). This analysis is habitually done in frequency domain (FD), but interest in time domain (TD) studies is gaining momentum. Commonly, TD solutions involve determining via Fourier transform techniques the configurational impulse response that is time-convolved with the excitation's signature. This approach may raise concerns about *causality*. First, the excitation is often noncausal (see the review in [6]). Second, the causality of the impulse response may be debatable when the used formulation cannot *a priori* guarantee the causality of the result or may be effectively lost when resorting to the discrete inverse Fourier transform [7, Ch. 11] or when the solution in the spectral domain is band-limited.

An effective alternative is resorting to the *intrinsically causal*, unilateral Laplace transform, with the TD inversion being effectuated through the Cagniard–de Hoop (**C-dH**) method [8]. This procedure was first used in antenna engineering in [9], was formalized in [10],
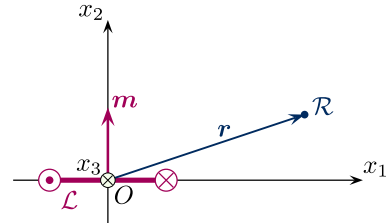
Fig. 1. Configuration consisting of a pulsed-fed, transmitting loop $\mathcal{L}$ with an equivalent magnetic moment $\boldsymbol{m}$. The pulsed radiated EM field is sensed at a receiving point $\mathcal{R}$ of position vector $\boldsymbol{r}$.

and has increasingly become the instrument of choice for exploring the pulsed EM field in layered configurations [11, Ch. 14]. At variance with the previously examined situation, all Green's functions yielded by the **C-dH** method are *rigorously causal*. By combining them with strictly causal excitations, the causality of the response is beyond any doubt. However, as with any formulation relying on the convolution of Green's function with an excitation, this approach may, and often does, suffer from a divergent behavior in the evaluation of the intervening integrals for (very) late times.

By starting from an illustrative example, this communication offers a solution for preventing the divergent late-time behavior of the convolution integrals combining causal Green's functions available at discrete time samples and causal excitations. The given example uses Green's function calculated via a typical **C-dH** formulation. First, the causes of the emergence of the divergent behavior will be scrutinized. A simple, yet extremely effective framework for guaranteeing the integrals' convergence will subsequently be put forward. The efficacy of the proposed method will be illustrated through numerical experiments, after which conclusions will be drawn.

II. ACCURACY CONCERNS IN THE EVALUATION OF CONVOLUTION INTEGRALS

A. Case Study

The present analysis builds upon convolution integrals derived for the configuration in Fig. 1. The position is specified by the coordinates $\{x_1, x_2, x_3\}$ with respect to a Cartesian reference frame. The time coordinate is t. The EM field is radiated by a current-carrying loop $\mathcal{L}$ centered at the origin and lying in the $x_2 = 0$ plane, and it is sensed at a receiving point $\mathcal{R}$ of position vector $\boldsymbol{r} = x_1\boldsymbol{i}_1 + x_2\boldsymbol{i}_2 + x_3\boldsymbol{i}_3$ (cylindrical symmetry allows confining the study to the $x_3 = 0$ plane). $\mathcal{L}$ radiates in an infinite embedding of permittivity ε_0, permeability μ_0, and wavespeed $c_0 = (\varepsilon_0\mu_0)^{-1/2}$. The pulsed feeding current $i(t)$ has a (conventional) pulsewidth t_w, the loop's diameter being small with respect to the pulse's spatial extent $c_0 t_\mathrm{w}$. Under this assumption, the radiating loop can be construed as a magnetic moment $\boldsymbol{m}(t) = i(t)A = i(t)A\boldsymbol{i}_3$, with A being the area enclosed by the loop $\mathcal{L}$.

The configuration in Fig. 1 was used in [12] for validating the therein derived **C-dH** methodology. The last step in that formulation required convolving the (semianalytically) evaluated (ray) Green's

functions with the causal excitation's signature. Upon taking a single-ray constituent in [12, eq. (47)] and ignoring some constants, the radiated E-polarized electric $\boldsymbol{E}(\boldsymbol{r}, t) = E_2(\boldsymbol{r}, t)\boldsymbol{i}_2$ and magnetic $\boldsymbol{H}(\boldsymbol{r}, t) = H_1(\boldsymbol{r}, t)\boldsymbol{i}_1 + H_3(\boldsymbol{r}, t)\boldsymbol{i}_3$ field strengths can be expressed as

$$\mathscr{V}(\boldsymbol{r}, t) = [g(\boldsymbol{r}, t)H(t - \tau_{\mathrm{a}})] \overset{(t)}{*} \partial_t^3 f(t)$$
$$= \int_{\tau = \tau_{\mathrm{a}}}^{t} \left[\partial_{t-\tau}^3 f(t - \tau)\right]\left[g(\boldsymbol{r}, \tau)\right]\mathrm{d}\tau \quad (1)$$

in which $\mathscr{V}(\boldsymbol{r}, t)$ stands for $E_2(\boldsymbol{r}, t)$, $H_1(\boldsymbol{r}, t)$, or $H_3(\boldsymbol{r}, t)$; τ_{a} is the ray's arrival time; $g(\boldsymbol{r}, t)$ is the ray's (modified) Green's function; $H(\cdot)$ is the Heaviside step function; $f(t)$ is the pulsed excitation; and $\overset{(t)}{*}$ denotes the time convolution. Note that this study focuses on the *temporal* behavior of signatures concerning *specified* locations. For simplicity, the explicit mentioning of $\boldsymbol{r}$ may be henceforth omitted in expressions where it is but an idle parameter.

For ensuring causality, the examples in [12] used $\partial_t \mathrm{PE}(\nu, t_{\mathrm{r}}, t)$ [see (10)] as excitation shape. An attractive alternative causal shape is the time-windowed $\partial_t \mathrm{WP}(\nu, t_{\mathrm{r}}, t)$ pulse of width $t_{\mathrm{w}} = 2t_{\mathrm{r}}$ [see (12)]. By taking $\nu \geqslant 5$, both the signatures are continuously differentiable up to, and including, their third time derivative at $t = 0$, as required by (1).

Comparing the **C-dH** solution for the mentioned $\partial_t \mathrm{PE}$ excitation with the corresponding analytical values derived in [13] for the configuration in Fig. 1 evidenced an unacceptably large discrepancy at late times. The discrepancy persisted, be it less pronounced, when using the $\partial_t \mathrm{WP}$ excitation (that should have yielded a zero field outside the pulses' support). Surprisingly, the deviation was substantially smaller when using a $\partial_t \mathrm{PE}$ excitation with $\nu = 7$. Since all these exercises used exactly the same Green's function, this erratic anomaly could only be attributed to the convolution integral.

The causes of this defect will be henceforth examined for the cases of time-windowed and infinite-tail excitations.

B. Time-Windowed Excitations

The $\partial_t \mathrm{WP}$ pulse is used as a typical time-windowed excitation shape. Its support is $[0, t_{\mathrm{w}}]$, with its integral over $[0, t_{\mathrm{w}}]$ being zero (see [14]). Furthermore, selecting $\nu \geqslant 5$ ensures beneficial continuous differentiability properties at $t = 0$ and $t = t_{\mathrm{w}}$, with $\partial_t \mathrm{WP}(0) = \partial_t \mathrm{WP}(t_{\mathrm{w}}) = 0$. By accounting for the finite support of $\partial_t \mathrm{WP}$, (1) becomes for $t > \tau_{\mathrm{a}} + t_{\mathrm{w}}$

$$\mathscr{V}(\boldsymbol{r}, t) = \int_{\tau = t - t_{\mathrm{w}}}^{t} \left[\partial_{t-\tau}^3 f(t - \tau)\right]\left[g(\boldsymbol{r}, \tau)\right]\mathrm{d}\tau \quad (2)$$

that becomes via successive integrations by parts

$$\mathscr{V}(\boldsymbol{r}, t) = \int_{\tau = t - t_{\mathrm{w}}}^{t} \left[f(t - \tau)\right]\left[\partial_\tau^3 g(\boldsymbol{r}, \tau)\right]\mathrm{d}\tau$$
$$- \sum_{k=0}^{2} \left[\partial_{t-\tau}^k f(t - \tau)\right]\left[\partial_\tau^{2-k} g(\boldsymbol{r}, \tau)\right]\Big|_{\tau = t - t_{\mathrm{w}}}^{t}. \quad (3)$$

Since $\partial_t \mathrm{WP}$ and its first three derivatives vanish at 0 and t_{w}, all terms under summation vanish implying that

$$\mathscr{V}(\boldsymbol{r}, t) = \int_{\tau = t - t_{\mathrm{w}}}^{t} \left[f(t - \tau)\right]\left[\partial_\tau^3 g(\boldsymbol{r}, \tau)\right]\mathrm{d}\tau. \quad (4)$$

Experience shows that $g(\boldsymbol{r}, \tau)$ becomes quickly extremely smooth, with $|g(\boldsymbol{r}, \tau)|$ increasing monotonically.[1] It can be safely assumed

that $g(\boldsymbol{r}, \tau)$ can be approximated over $[t - t_{\mathrm{w}}, t]$ as a third-order polynomial (in fact, a second-order polynomial also suffices). Under this assumption, (4) becomes

$$\mathscr{V}(\boldsymbol{r}, t) = \kappa \int_{\tau = 0}^{t_{\mathrm{w}}} \partial_t \mathrm{WP}(\nu, t_{\mathrm{r}}, \tau)\mathrm{d}\tau = 0 \quad (5)$$

with $\kappa \in \mathbb{R}$ some constant. Since the integral in (5) is zero, it can be concluded that for the considered degree of regularity of $g(\boldsymbol{r}, \tau)$, the convolution integral *must* be zero outside the support of the excitation, this also concurring with the behavior predicted by the expressions in [13].

However, in a computer code, $g(\boldsymbol{r}, \tau)$ is only determined at discrete time samples and, thus, the integral in (2) must be evaluated numerically. The inherent limited accuracy of any numerical integration scheme will then prevent the condition in (5) from being met even for a bounded integration interval and irrespective of the time step for sampling $g(\boldsymbol{r}, \tau)$. Moreover, upon noting that $|\partial_{t-\tau}^3 f(t - \tau)| < \mathscr{C}$ on $[0, t_{\mathrm{w}}]$, with $\mathscr{C} > 0$ being a real constant, the mean-value theorem for integrals entails that $|\mathscr{V}(\boldsymbol{r}, t)|$ given by (2) will vary as $t_{\mathrm{w}}\mathscr{C}|g(\boldsymbol{r}, \tau)|$ and, since $|g(\boldsymbol{r}, \tau)|$ is monotonically increasing for late times, the deviation will build-up with time, as evidenced by our experiments.

C. Infinite-Tail Excitations

The $\partial_t \mathrm{PE}$ pulse is used as a typical causal, infinite-tail excitation shape. Selecting $\nu \geqslant 5$ again entails beneficial continuous differentiability properties at $t = 0$, with $\partial_t \mathrm{PE}(0) = 0$. However, its prototype's expression [6] implies that only

$$\lim_{t \to \infty} \int_{\tau = 0}^{t} \partial_t \mathrm{PE}(\tau)\mathrm{d}\tau = 0 \quad (6)$$

with any finite t yielding a nonzero integral. In this case, too, an analysis as that in Section II-B is possible, with the additional restriction given by (6). The situation is further aggravated by the fact that the integration interval in (1) increases with time. It then follows that the deviation will increase with time much faster than in the case of the $\partial_t \mathrm{WP}$ excitation, as already indicated in Section II-A.

III. Accuracy and Effectiveness Improvement via Polynomial Approximation

The late-time error build-up in evaluating (1) can be precluded via a suitable polynomial interpolation/extrapolation.[2] Its effect differs depending on the type of excitation.

A. Time-Windowed Excitations

Assume that there exists an instant $\tilde{t}_{\mathrm{p}} > t_{\mathrm{w}}$ such that Green's function $g(\boldsymbol{x}', \tau)$ can be acceptably approximated for any t beyond $t_{\mathrm{p}} = \tau_{\mathrm{a}} + \tilde{t}_{\mathrm{p}}$ as a second-order polynomial

$$g(\boldsymbol{r}, \tau) \approx \mathscr{P}_2(\tau) = a_2\tau^2 + a_1\tau + a_0 \quad (7)$$

the coefficients a_0, a_1, and a_2 being inferred via polynomial regression (e.g., using the `polyfit` MATLAB function). Numerical experiments have shown that it suffices to take $\tilde{t}_{\mathrm{p}}$ as slightly larger than t_{w}, all examples in this communication making use of $\tilde{t}_{\mathrm{p}} = 1.2t_{\mathrm{w}} = 2.4t_{\mathrm{r}}$. With this choice, the evaluation of (1) differs depending on the time sample t.

---

[1] An elaborate examination of this property exceeds the scope of the present study. The reader is referred to [15, eq. (29)] for an illustration of this increase and to [10, eq. (92)] for the asymptotic behavior of the **C-dH** contour, both the results legitimating the monotonic increase in $|g(\boldsymbol{r}, \tau)|$.

[2] The present approach relies on distinguishing between different types of integrals ("partition") and using, where applicable, a polynomial approximation ("extrapolation"). By this token, it shares conceptual, although not technical, similarities with the formulation advocated in [3].

1) Evaluation at $t \in (\tau_a, t_p]$: The polynomial approximation is not applicable and (1) must be evaluated numerically. However, the integration interval is at most t_w long, the upper limit applying for $t \in [\tau_a + t_w, t_p]$. The quadrature is then accurate and fast—using precomputed values for the $\partial_{t-\tau}^3 f(t-\tau)$ part in (1) substantially expedites the computations.

2) Evaluation at $t \in (t_p, t_p + t_w]$: In this case, the polynomial approximation becomes partially available. Let now $t = t_p + t_w - \Delta_t$ with $0 \leqslant \Delta_t < t_w$. The integration in (1) is partitioned over $[t - t_w, t_p] \cup (t_p, t]$, with (7) being applicable over $(t_p, t]$. Successive integrations by parts will then yield

$$\mathscr{V}(\boldsymbol{r}, t) \approx \int_{\tau=t_p-\Delta_t}^{t_p} \left[\partial_{t-\tau}^3 f(t-\tau)\right]\left[g(\boldsymbol{r}, \tau)\right]\mathrm{d}\tau$$
$$+ \left(a_2 t_p^2 + a_1 t_p + a_0\right) \partial_t^2 f(t_w - \Delta_t)$$
$$+ \left(2a_2 t_p + a_1\right) \partial_t f(t_w - \Delta_t)$$
$$+ 2a_2 f(t_w - \Delta_t). \tag{8}$$

This expression is twice beneficial: The support of the integral that still needs being handled numerically shrinks to zero as $t \to t_p + t_w$, this forcing the integral to vanish. The remaining terms contain time derivatives of $\partial_t \mathrm{WP}(\nu, t_r, \tau)$ that also tend to zero for $\tau \to t_w$ (which, in fact, corresponds to the same $t \to t_p + t_w$). It can now be concluded that $|\mathscr{V}(\boldsymbol{r}, t)|$ in (8) drops to zero as $t \to t_p + t_w$ *irrespective of the possible inaccuracies induced by the numerical integration.*

3) Evaluation at $t > t_p + t_w$: The polynomial approximation applies now to the entire integration interval, implying that by substituting the *second-order* polynomial in (4), the expression of the convolution integral effectively vanishes. As a result, the evaluation of the convolution can be fully skipped, with evident computational benefits.

B. Infinite-Tailed Excitations

Although the $\partial_t \mathrm{PE}$ pulse has an infinite tail, it can be assigned a *conventional* pulsewidth t_w given by (14). Assume that there exists $\tilde{t}_p > t_w$ such that for $t > t_p = \tau_a + \tilde{t}_p$, Green's function can be expressed as in (7). For consistency with the time-windowed choice, all reported examples make use of $\tilde{t}_p = 2.4t_r$ that exceeds the value of t_w in (14).

1) Evaluation at $t \in (\tau_a, t_p]$: As in the case of $\partial_t \mathrm{WP}$ excitation, the polynomial approximation is not applicable and (1) must be evaluated numerically. At variance with the time-windowed case, the infinite tail of $\partial_t \mathrm{PE}$ yields a monotonically increasing integration interval that, in turn, results in longer computation times and, possibly, higher quadrature errors.

2) Evaluation at $t > t_p$: By making use of the notation $t = t_p + \Delta_t$ with $\Delta_t > 0$, the integral in (1) is partitioned in a manner that is reminiscent of (8) as

$$\mathscr{V}(\boldsymbol{r}', t) \approx \int_{\tau=\tau_a}^{t_p} \left[\partial_{t-\tau}^3 f(t-\tau)\right]\left[g(\boldsymbol{r}', \tau)\right]\mathrm{d}\tau$$
$$+ \left(a_2 t_p^2 + a_1 t_p + a_0\right) \partial_t^2 f(\Delta_t)$$
$$+ \left(2a_2 t_p + a_1\right) \partial_t f(\Delta_t) + 2a_2 f(\Delta_t). \tag{9}$$

The integral to be evaluated numerically is effectuated over an interval of fixed length $t_p - \tau_a$. Furthermore, $\left|\partial_t^k f(t)\right|$, $k = 0, \ldots, 3$, decay exponentially for $\partial_t \mathrm{PE}(\nu, t_r, t)$ beyond an instant t_{ed} that depends on ν and t_r. It then follows that the three supplementary terms will decay exponentially for $\Delta_t > t_{ed}$. Moreover, by observing that $t - \tau = \Delta_t + t_p - \tau$, it can be inferred that the integrand is sampled over a by Δ_t shifted $[\tau_a, t_p]$ interval and, then, $\partial_t^3 f(t-\tau)$

will also eventually start decaying exponentially. Summarizing, the expression in (9) contains a numerical integral of an exponentially decaying integrand and with a fixed length support, supplemented by three exponentially decaying analytic terms. This formulation clearly outperforms the direct integration.

Nonetheless, using the time-windowed $\partial_t \mathrm{WP}$ excitation is evidently superior: 1) the quantities used in that case for evaluating (1) drop rapidly to zero and become effectively zero beyond a certain instant, this eliminating the need of their calculation and 2) since $t_p > t_w$, the length of the interval over which the numerical quadrature must be performed is smaller, this being propitious from both computational time and accuracy points of view.

C. Discussion

The results derived in this section refer to convolutions of the type in (1), comprising a third-order time derivative of the excitation. Other formulations may yield expressions using different order derivatives, such as second order in [16, eq. (30)] or fourth-order in [16, eq. (23)]. Based on (8) and (9), the case of higher than third-order derivatives is readily covered by the discussed formalism, since fourth- and higher order derivatives of the considered (second-order) polynomial approximation vanish. Nonetheless, second- or lower order derivatives of the excitation require a separate study. Assuming the same order of Green's functions' polynomial approximation, such derivative orders will yield different supplementary terms in (8) and (9). However, the zero-value and exponential decay arguments will still hold and, hence, the inferred conclusions remain valid.

Another interesting point is that the **C-dH** contour becomes asymptotically a straight line (see [10, eq. (92)]). This convenient form allows an exact calculation of the Green's function *for very late times* and, thus, can form the basis of an analytic examination of the field representation's accuracy. At the same time, it offers a cogent support for the adopted second-order polynomial approximation of Green's function.

It is important to note that computational schemes that are not affected by any late-time error build-up have also been reported. For example, the convolution integral may be evaluated analytically in some particular cases [17], [18], while [11, Appendix H] demonstrated the virtues of the so-called "recursive convolution technique." Nevertheless, the framework in this section was specifically devised for situations when relevant Green's function is only available at discrete time samples. The applicability of the error-accumulation-free schemes to those situations is debatable and comparisons with them are intentionally left out.

To conclude with, this section demonstrated in a compelling manner how the late-time error build-up can be precluded for time-windowed excitations and, to a lesser degree, for causal but infinite-tail ones. However, none of the derived arguments applies to noncausal excitations, this raising additional concerns about the adequacy of such pulse shapes to TD studies, especially when late-time behavior is of particular interest.

IV. ILLUSTRATIVE NUMERICAL EXPERIMENTS

The (computational) opportunity of the framework assembled in Section III is now validated via illustrative numerical experiments. These experiments were conducted via a self-developed MATLAB code. For properly focusing on the algorithms' features and for being able to infer computational metrics, the code deliberately used only elementary quadrature via the MATLAB `trapz` function.

A. Computational Choices

The presented experiments make use of $\partial_t \mathrm{PE}$ and $\partial_t \mathrm{WP}$ excitations with pulse raising power $\nu = 5$. The plots are constructed for
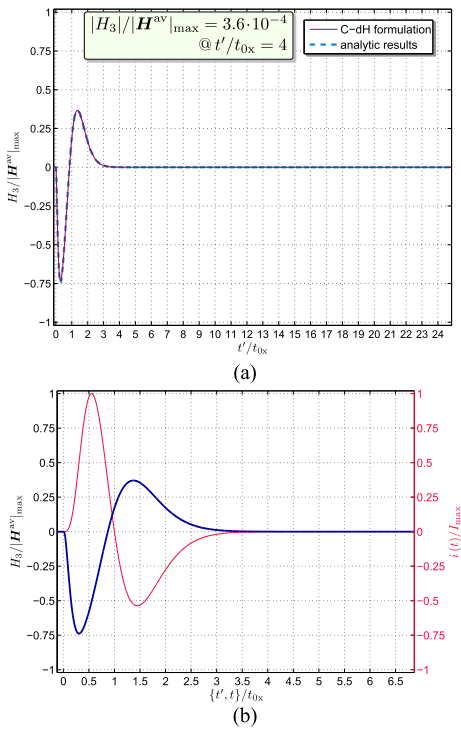
Fig. 2.   Normalized H_3 analysis for a ∂_tPE excitation with $\nu = 5$—present approach. (a) Comparison between the analytical and **C-dH**-evaluated values—T$_1$ analysis and (b) T$_2$ analysis—the exciting current pulse $i(t)$ of amplitude I_{max} is superimposed for reference.

Fig. 3.   Normalized H_3 analysis for a ∂_tWP excitation with $\nu = 5$—present approach. (a) T$_2$ analysis—the exciting current pulse $i(t)$ of amplitude I_{max} is superimposed for reference and (b) zoom-in corresponding to the end of the excitation's signature.

the normalized quantity $H_3/|\boldsymbol{H}^{av}|_{max}$ in which "av" stands for the "analytical values" given by the radiated field expressions in [13]. The abscissa variable is the by-the-arrival-time-retarded time coordinate $t' = t - \tau_a$, normalized by the zero-crossing time $t_{0x} = t_r$ (see Appendix A).

Two types of $H_3/|\boldsymbol{H}^{av}|_{max}$ signatures are examined: T$_1$, corresponding to $t' \in [0, 25]$ and intended for examining the convolution integral's behavior at very late times; T$_2$, corresponding to $t' \in [0, 7]$ and highlighting the "active" section of the pulsed field. While the T$_1$ time window may seem exaggerate, its use is justified by the relevance of examining the late-time ringing in layered configurations. One practical scenario would be for predicting the radiation from a CMOS-integrated, small loop that is fed by the monopulse generated with the circuitry introduced in [19]—its shape was shown in [20] to be an almost exact replica of the ∂_tWP pulse. The T$_1$ time window will then be adequate for studying pulse trains with a repetition frequency of $1\,\mathrm{GHz}$, as required by an ultrahigh data rate, near-field data transfer.

All reported signatures correspond to a receiving point located at $\boldsymbol{r} = x_1\boldsymbol{i}_1 + x_3\boldsymbol{i}_3$, with $x_1 = 4$ mm and $x_3 = 1$ mm (in accordance with the experiments reported in [12]). Since the examined configuration in Fig. 1 is in free space, no interface-induced reflections can appear and, thus, all the signatures are obtained via a single-ray evaluation of the **C-dH** strategy demonstrated in [12]. In all the reported experiments, the polynomial approximation was applied for $t \geqslant \tau_a + 2.4t_r$.

B. Infinite-Tail Excitations

A first experiment refers to the field radiated in the case of a ∂_tPE feeding. The corresponding T$_1$ signature is shown in Fig. 2(a) and clearly illustrates the vanishing tail. A similar behavior, not reported

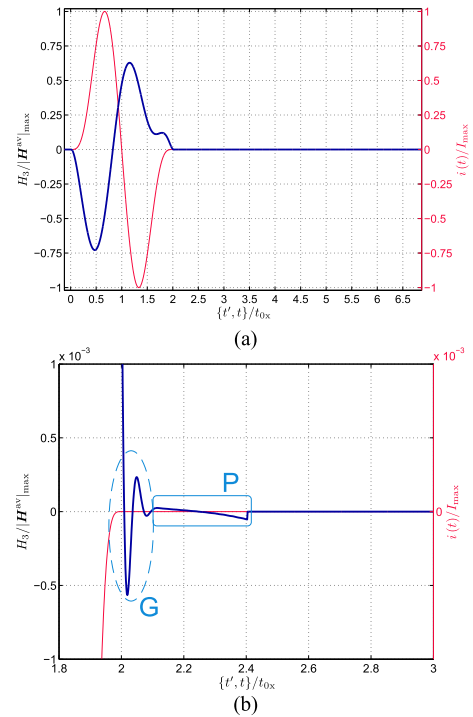here for brevity, was obtained in the case of a ∂_tPE excitation with $\nu = 7$. Upon noting that the strategy in Section III-B used different expressions for $t < t_p$ and $t > t_p$, it is important to examine possible computational artifacts that may appear in the transition zone. The T$_2$ study in Fig. 2(b) documents the smooth, artifact-free transition.

C. Time-Windowed Excitations

The second experiment refers to the field radiated in the case of ∂_tWP feeding. Since in this case the calculated field is effectively zero for $t > t_p + t_w$, a T$_1$ study is useless, with the assessment being confined to the possible computational artifacts in the transition zone. The corresponding T$_2$ signature is shown in Fig. 3(a) and confirms an artifact-free transition. For gaining confidence, a hugely zoomed-in plot of the transition is given in Fig. 3(b). Only at four orders of magnitude under the peak $|\boldsymbol{H}|$ become visible some discrepancies between the numerically integrated and polynomially approximated values (see the solid box P)! It is also worth mentioning that only at this level can one note the first vestiges of the inaccuracies in the computation of Green's function (the dashed ellipse G), this certifying the accuracy of the **C-dH** method.

D. Computational Metrics

The computational efficiency of the proposed formulation is now examined based on some computational metrics.

As a baseline, it is mentioned that the convolution integrals were evaluated via a function yielding all three components E_2, H_1, and H_3 for the complete set of time samples in an interval. The function used precomputed Green's function values but assembled internally all needed polynomial approximations and excitation signatures. The MATLAB code was run on a Windows 10, i7/2.60-GHz laptop. T$_1$ and T$_2$ signatures comprised 16 661 and 4661 time samples, respectively.
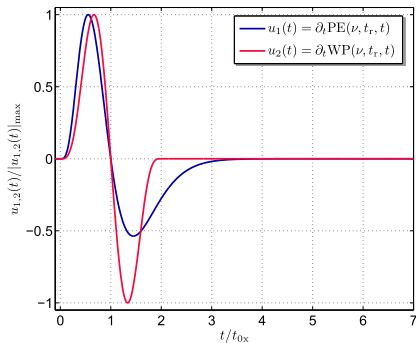
Fig. 4. Pulse shapes of $u_1(t) = \partial_t PE(5, t_r, t)$ and $u_2(t) = \partial_t WP(5, t_r, t)$.
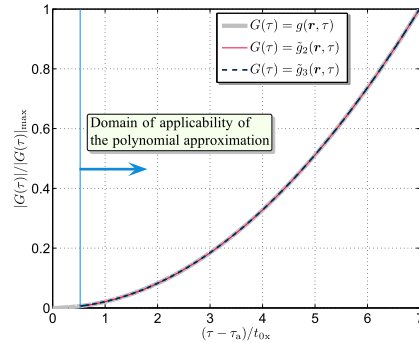

Fig. 5. Normalized Green's function corresponding to H_3 at $\mathbf{r} = 4\mathbf{i}_1 + \mathbf{i}_3$ (mm), and its polynomial replication. The abscissa variable is the normalized, by-the-arrival-time-retarded time coordinate $t' = \tau - \tau_a$. The domain of applicability of the polynomial approximation is highlighted.

The runtime for evaluating T_2 signatures amounted to 5.66 and 6.42 s for $\partial_t WP$ and $\partial_t PE$ excitations, respectively. As for T_1 signatures, constructing them required 50.25 s for a $\partial_t WP$ excitation and 54.61 s for a $\partial_t PE$ one. Recall that these computation times also include the assembling of the excitation samples. The huge number of time samples in T_1 allowed in that case to estimate the time required for calculating the excitation. Upon deducting that part, it was inferred that the net time for evaluating the convolution integrals with both Green's function and excitation having precomputed values amounted to approximately 8 and 20 s for the $\partial_t WP$ and $\partial_t PE$ excitations, respectively. These runtimes concur with the fact that calculating the field values is skipped for the $\partial_t WP$ excitation when $t > t_p + t_w$.

This analysis cogently shows that the proposed strategy is not only accurate but also computationally highly effective.

V. Conclusion

A decidedly accurate and computationally effective strategy for dealing with the tail of the convolution integrals involving strictly causal excitations was demonstrated. The method was shown to perform superiorly with time-windowed excitations, with the expected zero tail being replicated with a seamless transition between regions where different evaluation models were used. The technique is of interest for a wide range of TD EM problems yielding a convolution between a function available at discrete time samples and a (time-differentiated) excitation. Its implementation is effortless, requiring only a choice for the order of the function's polynomial approximation, and an (empiric) determination of the start of the interval where this approximation applies. As a rule, the polynomial interpolation should be at least one order lower than the time derivative applying to the excitation. Furthermore, using time-windowed feeding is clearly recommendable.

Appendix

A. Excitation Pulse Shapes

For ensuring the causality requirement, this communication uses exclusively causal excitations pulse shapes, namely, as follows.

1) Time-Differentiated Power-Exponential (PE) Pulse [6]:

$$\partial_t PE(v, t_r, t) = N_{PE} \left(1 - t'\right) t'^{v-1} \exp\left[-v \left(t' - 1\right)\right] H(t) \quad (10)$$

in which $v = 2, 3, 4, \ldots$ is the pulse rising power, $t_r > 0$ is the pulse rise time, $t' = t/t_r$, $H(\cdot)$ is the Heaviside step function, and N_{PE} is a normalization parameter that reads

$$N_{PE} = v^{v/2} \left(v^{1/2} - 1\right)^{1-v} \exp\left(-v^{1/2}\right). \quad (11)$$

2) Time-Differentiated Windowed-Power (WP) Pulse [14]:

$$\partial_t WP(v, t_r, t) = N_{WP} t'^{v-1} (2 - t')^{v-1} H(t') H(2 - t') \quad (12)$$

in which the normalization parameter N_{WP} reads

$$N_{WP} = 2^{1-v} (v - 1)^{1-v} (2v - 1)^{v-1/2}. \quad (13)$$

Both the pulses are inferred from prototype *unipolar* pulses via time differentiation and are normalized to a unit amplitude. The pulse rise time is taken as the interval between the onset and the instant when the corresponding unipolar pulse peaks. The signatures given by (10) and (12) have zero-crossings at $t_{0x} = t_r$. By taking $v \geqslant 5$, they are continuously differentiable up to, and including, their third time derivative at $t = 0$, this feature applying for $\partial_t WP$ at $t = t_w$, as well. The $\partial_t WP$ pulse is time-windowed and has the pulsewidth $t_w = 2t_r$ [14]. Although the $\partial_t PE$ pulse has an infinite tail, it can be assigned a *conventional* pulsewidth that follows by applying [6, eq. (23)] to its prototype unipolar pulse and amounts to:

$$t_w = t_r \, \Gamma(v + 1) \exp(v) / v^{v+1} \quad (14)$$

with $\Gamma(\cdot)$ denoting the Euler gamma function. Note that $t_w < 1.85 t_r$ for $v \geqslant 2$. Both model pulses have analytical Fourier transforms [6], [14]. The $\partial_t PE$ and $\partial_t WP$ shapes used in this communication are shown in Fig. 4. Their spectral behaviors peak at $0.283/t_r$ and $0.441/t_r$, respectively, and fall by 20 dB/decade toward zero and by about 100 dB/decade toward infinity.

B. Green's Function Analysis

Application of the **C-dH** method [8] to EM problems concerning stratified media yields the solution as a convolution between a (higher order) *time derivative* of the excitation's signature and Green's function. In the specific situation examined in [12], that solution is, apart from some constants, of the form (see [12, eq. (47)])

$$\mathscr{V}(\mathbf{r}, t) = \int_{\tau = \tau_a}^{t} \left[\partial_{t-\tau}^3 f(t - \tau)\right] \left[g(\mathbf{r}, \tau)\right] d\tau \quad (15)$$

with all intervening quantities being defined in Section II-A. As in most **C-dH** frameworks, $g(\mathbf{r}, \tau)$ is obtained at discrete time samples, only. This communication uses free-space Green's function, its shape at the location used in Section IV-A being shown in Fig. 5. This $g(\mathbf{r}, \tau)$ can be accurately replicated via third- or even second-order polynomials, their coefficients being inferred via polynomial regression (the present formulation uses the `polyfit` MATLAB

function). The relevant polynomial approximations are superposed in Fig. 5 on original Green's function. The representation error

$$\text{Err} = \left[\int_{\mathscr{T}} \big| g(\boldsymbol{r}, \tau) - \tilde{g}_m(\boldsymbol{r}, \tau) \big| \mathrm{d}\tau \right] \left[\int_{\mathscr{T}} \big| g(\boldsymbol{r}, \tau) \big| \mathrm{d}\tau \right]^{-1} \quad (16)$$

amounted to 0.1% and 0.02% in the case of the third- and second-order polynomial approximations, respectively, with $\tilde{g}_m(\boldsymbol{r}, \tau)$, $m = 3, 2$, denoting the polynomial replicas and $\mathscr{T}$ the interval over which they were calculated.

REFERENCES

[1] K. A. Michalski, "Extrapolation methods for Sommerfeld integral tails," *IEEE Trans. Antennas Propag.*, vol. 46, no. 10, pp. 1405–1418, Oct. 1998.

[2] J. Mosig, "The weighted averages algorithm revisited," *IEEE Trans. Antennas Propag.*, vol. 60, no. 4, pp. 2011–2018, Apr. 2012.

[3] K. A. Michalski and J. R. Mosig, "Efficient computation of Sommerfeld integral tails–methods and algorithms," *J. Electromagn. Waves Appl.*, vol. 30, no. 3, pp. 281–317, Feb. 2016, doi: 10.1080/09205071.2015.1129915.

[4] A. Sommerfeld, "Über die ausbreitung der wellen in der drahtlosen telegraphic," *Ann. Phys.*, vol. 4, no. 28, pp. 665–736, 1909.

[5] W. C. Chew, *Waves and Fields in Inhomogeneous Media*. Piscataway, NJ, USA: IEEE Press, 1995.

[6] I. E. Lager, A. T. de Hoop, and T. Kikkawa, "Model pulses for performance prediction of digital microelectronic systems," *IEEE Trans. Compon., Packag., Manuf. Technol.*, vol. 2, no. 11, pp. 1859–1870, Nov. 2012.

[7] R. N. Bracewell, *The Fourier Transform and its Applications*. Boston, MA, USA: McGraw-Hill, 2000.

[8] A. T. de Hoop, "A modification of Cagniard's method for solving seismic pulse problems," *Appl. Sci. Res. B*, vol. 8, no. 1, pp. 349–356, Dec. 1960.

[9] A. T. de Hoop, "Pulsed electromagnetic radiation from a line source in a two-media configuration," *Radio Sci.*, vol. 14, no. 2, pp. 253–268, Mar./Apr. 1979.

[10] M. Štumpf, A. T. De Hoop, and G. A. E. Vandenbosch, "Generalized ray theory for time-domain electromagnetic fields in horizontally layered media," *IEEE Trans. Antennas Propag.*, vol. 61, no. 5, pp. 2676–2687, May 2013.

[11] M. Štumpf, *Time-Domain Electromagnetic Reciprocity in Antenna Modeling*. Hoboken, NJ, USA: Wiley, 2019.

[12] I. E. Lager, V. Voogt, and B. J. Kooij, "Pulsed EM field, close-range signal transfer in layered configurations—A time-domain analysis," *IEEE Trans. Antennas Propag.*, vol. 62, no. 5, pp. 2642–2651, May 2014.

[13] I. E. Lager and A. T. De Hoop, "Loop-to-loop pulsed electromagnetic field wireless signal transfer," in *Proc. 6th Eur. Conf. Antennas Propag. (EUCAP)*, Mar. 2012, pp. 786–790.

[14] I. E. Lager and S. L. van Berkel, "Finite temporal support pulses for EM excitation," *IEEE Antennas Wireless Propag. Lett.*, vol. 16, pp. 1659–1662, 2017.

[15] M. Stumpf and A. T. de Hoop, "Loop-to-loop pulsed electromagnetic signal transfer across a thin metal screen with Drude-type dispersive behavior," *IEEE Trans. Electromagn. Compat.*, vol. 60, no. 4, pp. 885–889, Aug. 2018.

[16] M. Stumpf, G. Antonini, I. E. Lager, and G. A. E. Vandenbosch, "Pulsed electromagnetic field signal transfer across a thin magneto-dielectric sheet," *IEEE Trans. Electromagn. Compat.*, vol. 63, no. 4, pp. 1058–1064, Aug. 2021.

[17] M. Stumpf, G. Antonini, I. E. Lager, and G. A. E. Vandenbosch, "Time-domain electromagnetic-field transmission between small-loop antennas on a half-space with conductive and dielectric properties," *IEEE Trans. Antennas Propag.*, vol. 68, no. 2, pp. 938–946, Feb. 2020.

[18] M. Stumpf and I. E. Lager, "On the excitation of anomalous EM transients along the surface of a thin highly contrasting sheet with dielectric and conductive properties," *IEEE Antennas Wireless Propag. Lett.*, vol. 20, no. 1, pp. 58–62, Jan. 2021.

[19] D. Pepe, L. Aluigi, and D. Zito, "Sub-100 ps monocycle pulses for 5G UWB communications," in *Proc. 10th Eur. Conf. Antennas Propag. (EuCAP)*, Apr. 2016, pp. 1–4.

[20] I. E. Lager and D. Zito, "Pulsed EM field radio: The low-power, ultra-fast bridge to ubiquitous fiber networks," in *Proc. 13th EuCAP*, Mar./Apr. 2019, pp. 1–5.